SUPPORTING INFORMATION: Resource-efficient digital quantum simulation of d-level systems for photonic, vibrational, and spin-s Hamiltonians.

Nicolas P. D. Sawaya,[1,*] Tim Menke,[2,3,4] Thi Ha Kyaw,[5,6] Sonika Johri,[7] Alán Aspuru-Guzik,[5,6,8,9] and Gian Giacomo Guerreschi[1,†]

[1] *Intel Labs, Santa Clara, California 95054, USA*
[2] *Department of Physics, Harvard University, Cambridge, MA 02138, USA*
[3] *Research Laboratory of Electronics, Massachusetts Institute of Technology, Cambridge, MA 02139, USA*
[4] *Department of Physics, Massachusetts Institute of Technology, Cambridge, MA 02139, USA*
[5] *Department of Computer Science, University of Toronto, Toronto, Ontario M5S 2E4, Canada*
[6] *Department of Chemistry, University of Toronto, Toronto, Ontario M5G 1Z8, Canada*
[7] *Intel Labs, Hillsboro, Oregon 97124, USA*
[8] *Vector Institute for Artificial Intelligence, Toronto, Ontario M5S 1M1, Canada*
[9] *Canadian Institute for Advanced Research, Toronto, Ontario M5G 1Z8, Canada*

CONTENTS

I. UPPER BOUNDS FOR ENTANGLING GATES

The number of required quantum operations is closely related to the lengths of the Pauli strings in the encoded Hamiltonian. The distribution of lengths of Pauli strings may be analyzed in terms of binomial distributions, because the quantity to be analyzed is a product of two-term sums, *i.e.* each $|x_i\rangle\langle x_i'|_i$ in the expression

$$|l\rangle\langle l'| \mapsto \bigotimes_{i\in C(l)\cup C(l')} |x_i\rangle\langle x_i'|_i \tag{1}$$

is mapped to a sum of exactly two one-qubit unitary operators, as outlined in the main text. Consequently, for a diagonal term $|l\rangle\langle l|$ the number of occurrences of length-p Pauli strings is

$$f_{|l\rangle\langle l|}(p;K) = \binom{K}{p}, \tag{2}$$

where K is $|C^{\mathrm{enc}}(l)\cup C^{\mathrm{enc}}(l')|$, *i.e.* the number of qubits in the relevant bitmask subsets. This is because every term in equation (1) is $|0\rangle\langle 0|$ or $|1\rangle\langle 1|$, which respectively map to $\frac{1}{2}(I+\sigma_z)$ and $\frac{1}{2}(I-\sigma_z)$. Hence all terms in the product have a single identity—consider *e.g.* $(I+\sigma_z)(I-\sigma_z)\cdots(I+\sigma_z)$—which leads to the Pauli string lengths having a binomial distribution.

We consider a Hermitian term $\alpha|l\rangle\langle l'| + \alpha^*|l'\rangle\langle l|$ where $l \neq l'$. For such a term, the resulting Pauli operator for this simple term pair will also be related to the binomial distribution. The number f of occurrences of length-p Pauli strings is

$$f(p;d_H,K) = \frac{1}{2}2^{d_H}\binom{K-d_H}{p-d_H}, \tag{3}$$

where $d_H = d_H(\mathcal{R}(l),\mathcal{R}(l'))$ and $\mathcal{R}$ depends on the chosen encoding. The reason for the $\frac{1}{2}$ factor is that non-Hermitian terms (*i.e.* Pauli strings with an imaginary coefficient) cancel out when we consider the sum $\alpha|l\rangle\langle l'| + \alpha^*|l'\rangle\langle l|$. The non-Hermitian term $|l\rangle\langle l'|$ would not have the $\frac{1}{2}$ factor when considering the distribution of Pauli string lengths, but we do not analyze such terms because the goal is to exponentiate Hermitian operators using quantum circuits.

It is conceptually useful to consider the case of all bits being mismatched, *i.e.* when $d_H = K$ for a term $\alpha|l\rangle\langle l'| + \alpha^*|l'\rangle\langle l|$. In this case, because there are no identity matrices present in the original product of equation (1), there are $\frac{1}{2}2^{d_H}\binom{K}{0} = 2^{d_H-1}$ Pauli strings, all with length K.

Combining equation (3) with $n_{\mathrm{cx}}(p) = 2(p-1)$ from equation (19) in the main text, an upper bound (denoted UB) for the number of CNOT gates is therefore

* nicolas.sawaya@intel.com
† gian.giacomo.guerreschi@intel.com

$$
\begin{aligned}
n_{\mathrm{cx,UB}}[d_H(l,l'),K] &= \sum_{p=2}^{K} f(p;d_H,K)(2p-2) \\
&= \frac{1}{2}\sum_{p=2}^{K} 2^{d_H}\binom{K-d_H}{p-d_H}(2p-2),
\end{aligned}
\tag{4}
$$

where the sum starts at $p = 2$ because CNOT gates are required only for $p > 1$. This is an upper bound because gate cancellations are possible once the circuit has been constructed.

Using known binomial identities given below, and again considering only the term $\alpha|l\rangle\langle l'| + \alpha^*|l'\rangle\langle l|$ or the diagonal $|l\rangle\langle l|$, this becomes (duplicated in the main text)

$$
\begin{aligned}
n_{\mathrm{cx,UB}}[d_H = 0,K] &= (2^K K - 2(2^K) - 2), \\
n_{\mathrm{cx,UB}}[d_H = 1,K] &= \frac{1}{2}(2^K K - 2^K), \\
n_{\mathrm{cx,UB}}[d_H = 2,K] &= \frac{1}{2}(2^K K).
\end{aligned}
\tag{5}
$$

The special case of $d_H = 0$ represents a diagonal term $|l\rangle\langle l|$. In the case of compact codes (standard binary and Gray) for which $\log_2 d$ is an integer, these formulas can be expressed in terms of the number of levels d as

$$
\begin{aligned}
n_{\mathrm{cx,UB}}[d_H = 0,K] &= d\log_2 d - 2d - 2, \\
n_{\mathrm{cx,UB}}[d_H = 1,K] &= \frac{1}{2}(d\log_2 d - 2d), \\
n_{\mathrm{cx,UB}}[d_H = 2,K] &= \frac{1}{2}d\log_2 d.
\end{aligned}
\tag{6}
$$

We derived formulas (5) from the following binomial identities

$$
\sum_{j}^{K}\binom{K}{j} = 2^K \tag{7}
$$

$$
\binom{K}{j} = \frac{K}{j}\binom{K-1}{j-1} \tag{8}
$$

$$
\binom{K}{j} = \frac{K(K-1)}{j(j-1)}\binom{K-2}{j-2}. \tag{9}
$$

Again, thus far we have considered upper bounds only for one term $\alpha|l\rangle\langle l'| + \alpha^*|l'\rangle\langle l|$ or one element $|l\rangle\langle l|$.

We now consider upper bounds for typical full matrix operators using a compact code. Equation (6) implies that for each term $\alpha|l\rangle\langle l'| + \alpha^*|l'\rangle\langle l|$, $n_{\mathrm{cx,UB}}$ is of order $O(d\log d)$. Hence, for the sparsity pattern of $\hat{B}$ discussed in the main text—for which the number of non-zero entries in the operator is $O(d)$—the compact encodings (Gray and SB) yield an upper bound of $O(d)O(d\log d)$=$O(d^2\log d)$ entangling gates.

On the other hand, equation (5) shows that for the unary encoding, one term pair $\alpha|l\rangle\langle l'| + \alpha^*|l'\rangle\langle l|$ has $n_{\mathrm{cx,UB}} \sim O(1)$, since the number of CNOT gates is independent of d. For sparsity pattern $\hat{B}$ this gives upper bounds of $n_{\mathrm{cx,UB}} \sim O(d)$, substantially less asymptotically than the compact encodings. This improved bound comes at the cost of the unary and BU encodings requiring more qubits.

For an operator corresponding to a *dense* matrix of $O(d^2)$ nonzero entries and represented with a compact encoding, the worst-case scaling would be $O(d^2)O(d\log d)$=$O(d^3\log d)$, but this is clearly an overestimate. In fact, there are only $O(4^{\log_2 d}) = O((2^{\log_2 d})^2) = O(d^2)$ distinct Pauli strings for $\log_2 d$ qubits and each of them requires at most $O(\log d)$ CNOT gates, for a total of $O(d^2\log d)$ entangling gates (this is the absolute limit based on counting and implementing all possible Pauli operators of length $\log_2 d$). As noted in the main text, the result is that the unary code has a diminished advantage as the density of the matrix operator increases.

Finally, in the block unary encoding for one Hermitian pair, the bitmask subset union has $K \sim O(\log g)$ bits, resulting in $O(g \log g)$ operations, in analogy to the compact case. Hence, sparsity pattern $\hat{B}$ yields a bound of $O(dg \log g)$ and a dense matrix yields $O(d^2 \log g)$.

In many cases these analytical expressions will not be particularly useful in calculating which encoding is best for a given operator, except to explain general trends. When including all terms in the matrix operator, there will be many repeated Pauli matrices whose coefficients will be summed, often leading to a reduction in the number of terms. Circuit optimizers, like the one used in this work, should also be used for more accurate resource estimates.

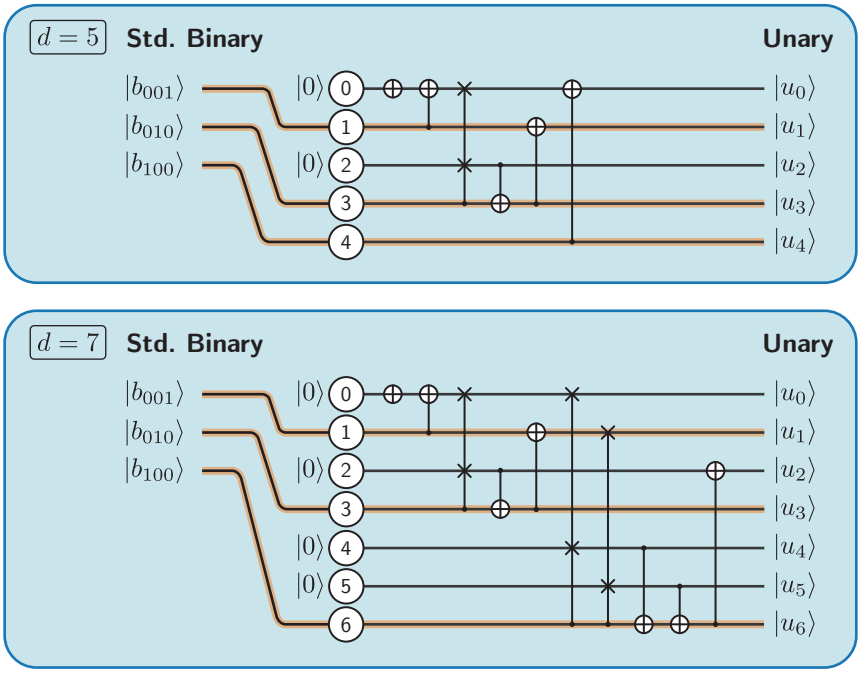

Supplementary Figure 1. Standard binary to unary conversion circuits for $d = 5$ and $d = 7$.

II. CIRCUIT OPTIMIZATION

The number of required two-qubit entangling gates (CNOT gates) per Suzuki-Trotter step was determined as follows. Each d-level operator was converted to a Pauli operator using the procedure of the main text. Collecting coefficients and cancelling Pauli terms was done using the `QubitOperator` class of the python software packages FermiLib and OpenFermion [MSK+17]. Pauli terms were listed in a pseudo-alphabetical order, such that all terms containing $\sigma_x^{(0)}$ are listed first, followed by terms beginning in $\sigma_y^{(0)}$, $\sigma_z^{(0)}$, $\sigma_x^{(1)}$, $\sigma_y^{(1)}$, etc. Quantum circuits were first synthesized by converting each Pauli term to a CNOT ladder, in the order described. One can see by inspection that circuit reductions will often occur. Pairs of CNOT, Hadamard, or $iR_{x+y}(\pi)$ gates, which appear after placing CNOT ladders next to each other, can be eliminated as they cancel to unity.

The circuit optimization was performed as follows. In the optimizer, every gate is represented in a data structure that contains its attributes, *e.g.* its inverse gate, its commutation properties with other gates, and whether it is a rotation gate. For each gate, the optimizer looks for an opportunity to cancel it with its inverse or merge it with another rotation gate by commuting it as far forwards and backwards as possible. The optimizer also looks for a limited set of commonly occurring patterns that allow for gate reductions. For the circuits used in this study, this pattern-searching allows us to reduce some sets of three CNOT gates to two: any gate sequence CNOT(i_0,i_1) × CNOT(i_1,i_2) × CNOT(i_0,i_1) is changed to the equivalent CNOT(i_0,i_2) × CNOT(i_1,i_2). Merging and cancelling gates, as well as this pattern-searching, are performed for several passes until the circuit converges.

The choice of ordering for the Pauli terms affects the gate counts, as different orderings of CNOT ladders affect the presence of particular pairs of eliminable gates. Finding the absolute optimal ordering is a combinatorially hard problem and is not the focus of this work [BKM18]. However, to test the quality of the default ordering, we took the encoded bosonic $\hat{q}$ operator for the unary, gray, and standard binary codes, testing >900 random orderings for each.

We found that the default ordering was superior to every random ordering. This result is intuitive, as orderings that match similar Pauli strings side-by-side will lead to more pairs of adjacent CNOT gates and adjacent single-qubit gates.

III. SB TO UNARY CONVERSION: GENERAL CASE

Here we discuss how to modify the SB-to-unary circuit shown in the main text when d is not a power of two. First, we shift the most significant SB qubit up to qubit $d-1$ rather than keeping it at qubit 2^K-1, where K is the number of qubits required by the standard binary encoding. Second, we change the control qubit of SWAP and CNOT gates from 2^K-1 to $d-1$, and remove all unnecessary qubits. Third, the target for the final CNOT is shifted up by the number of qubits that was removed. For instance, using $d=5$, the binary base line is shifted from **7** to **4**. We then remove qubits **4** through **6** and any associated gates. All SWAP and CNOT controlled by **7** become controlled by **4**. Finally, the last CNOT is placed with control **4** and target **0**. The latter target has index $d-1-2^{K-1}$. Examples for $d=5$ and 7 are given in Supplementary Figure 1. Algorithm 1 in the main text correctly implements these cases; the examples discussed here are shown only as a pedagogical aid.

IV. SB TO $\mathrm{BU}^{SB}_{g=3}$ CONVERSION

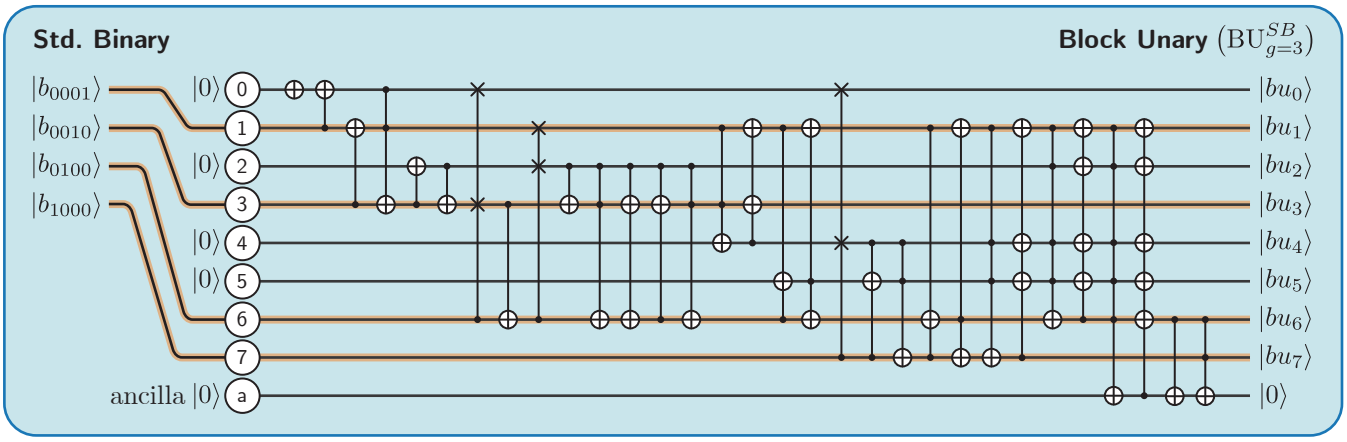

Supplementary Figure 2. Quantum circuit for standard binary to block unary ($\mathrm{BU}^{SB}_{g=3}$) conversion.

To show that one may in principle convert between all encodings, we provide a circuit for converting between SB and $\mathrm{BU}^{SB}_{g=3}$ with $d=12$. We do not write down the general case for this circuit, because the rare hardware budgets for which BU might be useful would likely be cases for which the hardware's gate count constraints would not allow for the cost of conversion.

V. FIRST QUANTIZATION

First quantized operators can be used to represent any bosonic degree of freedom because first quantized QHO operators obey bosonic algebra [MSAH18b, MSAH18a]. The utility of this approach comes partly from the fact that one can qssuickly move between the position and momentum bases by using the quantum Fourier transform, using a first quantized momentum operator $\tilde{P}_{\mathrm{FQ}}$ that is the direct analog of $\tilde{X}_{\mathrm{FQ}}$. For instance, consider implementing one Trotter step of an operator proportional to the approximate quantum harmonic oscillator Hamiltonian

$$\tilde{H}_{\mathrm{QHO}} \propto \tilde{X}^2_{\mathrm{FQ}} + \tilde{P}^2_{\mathrm{FQ}}. \tag{10}$$

One may first exponentiate $\tilde{X}^2$, then apply the quantum fourier transform (QFT) to move to the momentum basis, then apply $\tilde{P}^2$, and finally use QFT^{-1} to move back to the position basis. This allows for all the operations to be done

in the diagonal basis except for QFT, which takes just $O(N_q^2) \sim O(\log^2 d)$ operations. The Trotterization of $\tilde{X}_{\mathrm{FQ}}$ and $\tilde{P}_{\mathrm{FQ}}$ requires only $\log_2 d$ single-qubit rotations and zero two-qubit gates, as explained in the main text, although exponentiating their squares does require entangling gates.

However, a significant computational hurdle to the first quantization method is initial state preparation. Preparing the ground state of the QHO, for example, requires that one prepares the state

$$|\psi\rangle = \sum_{j=0}^{K-1} f(x_j)|x_j\rangle \tag{11}$$

where $f(x)$ would be a normalized Gaussian, the first Hermite-Gauss function. Macridin et al. discuss existing options for preparing such an arbitrary state [MSAH18a], showing that a variational approach is more efficient than one might expect for preparing ground states on near- or medium-term quantum computers. We expect that most early simulations of bosonic degrees of freedom on qubit-based quantum computers will use the Fock-type (*i.e.* second quantization) mappings that are the focus of the current work, since preparing a Fock state in second quantization is trivially done by flipping individual bits. However, there may be instances in which Fock states are not used, such as wave packet dynamics or other approaches, and it may be that there are other operator-based advantages in using the first quantization mapping. Note that the procedure for mapping $\tilde{X}$ and $\tilde{P}$ to qubits is no different than mapping any other matrix representation, with d replaced by N_x.

VI. HAMILTONIAN DEFINITIONS

In this section we provide the Hamiltonians studied in this work and discuss their relevance.

Bose-Hubbard model. The Bose-Hubbard model is a ubiquitous model in condensed matter physics, consisting of a set of bosonic modes that occupy discrete lattice sites. The phase diagram of the basic model consists of the Mott insulator and superfluid phases [FWGF89]. Adding additional terms such as increasing the interaction radius or introducing an effective magnetic field can give rise to more complex phases like a density wave phase and a supersolid phase [SJG10, LGHL18, LDML08]. The model has been experimentally realized in ultracold atomic lattices [BDZ08]. Recent experiments [TLF+19, BSW+19, CPI+19] report evidence for the creation of one of the more exotic predicted phases, a supersolid, a state of matter where an ordered material can flow without friction.

Simulating Bose-Hubbard models on a quantum computer will help elucidate the properties of these phases and possibly lead to the discovery of previously unknown phases. Quantum simulation may be especially important for studying behavior near the boundaries of quantum phase transitions, a regime that is notoriously difficult to study numerically on classical computers [HW17].

Here, we consider the 1D Bose-Hubbard model with periodic boundary conditions, expressed as

$$\hat{H}_{\mathrm{BH}} = -t\sum_{i}^{N}(\hat{a}_i^\dagger \hat{a}_{i+1} + h.c.) + \frac{U}{2}\sum_{i}^{N}\hat{n}_i(\hat{n}_i - 1) - \mu\sum_{i}^{N}\hat{n}_i \tag{12}$$

where t is the hopping term, U is the on-site site energy, and μ is the chemical potential. The parameters dictating the size of the problem are the number of levels d per site as well as the number of particles N.

Shifted one-dimensional QHO. We consider this Hamiltonian because it is one of the simplest prototypes for encoding a bosonic system into qubits. The Hamiltonian is directly relevant to chemistry, where it is equivalent to calculating the Franck-Condon factors [MMS+19, SH19] between two electronic transitions for a diatomic molecule. Franck-Condon factors determine the intensity of the transitions to vibrational eigenstates in the final electronic state. The Hamiltonian is

$$\hat{H}_{\mathrm{1D\ Shift}} = \frac{\omega}{2}[(\hat{q} - \delta)^2 + \hat{p}^2] \tag{13}$$

where ω is the QHO frequency and δ is the displacement (related to the commonly used Huang-Rhys factor). The parameter δ indirectly determines how many levels d will have appreciable intensity when considering overlaps with the unshifted QHO.

Multidimensional Franck-Condon factors. In the field of physical chemistry, in order to calculate an absorption spectrum, energy transfer characteristics, or other properties for molecules larger than two atoms, Franck-Condon profiles must include transitions to all possible vibrational Fock states of non-negligible intensity. Each vibrational normal mode in the final electronic state is a separate bosonic mode, and there are $M = 3N - 6(5)$ such modes in nonlinear (linear) molecules. One defines $\vec{q}_s$ and $\vec{p}_s$ to be vectors of position and momentum operators, respectively,

where s is one of two electronic potential energy surfaces (PESs) A or B. See references [Huh11, HGP+15, SH19] for more details. The unitary M-by-M Duschinsky matrix $\mathbf{S}$ transforms between the bases of the two PESs such that

$$\begin{aligned} \vec{q}_B &= \mathbf{\Omega_B S \Omega_A^{-1}} \vec{q}_A + \vec{\delta} \\ \vec{p}_B &= \mathbf{\Omega_B^{-1} S \Omega_A} \vec{p}_A \end{aligned} \tag{14}$$

where $\mathbf{\Omega}_s = diag([\omega_{s1}, ..., \omega_{sM}])^{\frac{1}{2}}$ and $\{\omega_{si}\}$ are vibrational modes of PESs. The Hamiltonian to simulate is

$$\hat{H}_{\text{FC}} = \frac{1}{2} \sum_j^M \omega_{Bj} (q_{Bj}^2 + p_{Bj}^2) \tag{15}$$

In the multidimensional case, all four parameters $\vec{\delta}$, $\mathbf{S}$, $\mathbf{\Omega_A}$, and $\mathbf{\Omega_B}$ indirectly determine the bosonic truncation in each mode, out of which the dimensionless displacement $\vec{\delta}$ usually has the greatest effect. Depending on these parameters, the required d in a given mode can be anywhere from 1 in the case of negligible shifts, to as high as 70 in molecules such as nitrogen dioxide [SH19]. Though we consider the harmonic case here, it is the anharmonic Hamiltonians, where higher-order Taylor series terms are added to (15), where a quantum computer will likely first outperform a classical one for small molecules [SH19, LKC06, HNRB10, MR15, PR17].

For real molecules, the Duschinsky matrix $\mathbf{S}$ tends to be sparse. In our resource count simulations, we assume that each row of $\mathbf{S}$ has a constant number of non-zero entries per row, k. We set $k = 4$ for the simulations discussed here. We additionally assume that each vibrational mode is modelled with the same number of levels d, though for most real molecules one would use a different d for each mode. We make the approximations in order to compare typical constant-factor savings between different mappings, independent of system size.

Spin-s Heisenberg model. Quantum Heisenberg models, commonly used to study theoretical questions in condensed matter physics and to model magnetism in real solids, consist of quantum spins placed on a lattice. Though most work has focused on spin-$\frac{1}{2}$ particles, some problems require the use of higher-spin systems. Interpreting nuclear magnetic resonance experiments [Lev08] can require modeling higher-spin systems. Notably, a Heisenberg model simulation using a high spin of spin-$\frac{7}{2}$ has been recently reported [LSGB+16], where the magnetic properties of the material $GdRhIn_5$ are studied. There are many stable isotopes up with nuclear spin $I = \frac{7}{2}, 4, \frac{9}{2}$ [Sto05], and with unstable isotopes reaching still higher I.

For this work, we consider a one-dimensional spin-s Heisenberg model with ferromagnetic $\hat{S}_z \hat{S}_z$ interactions and a magnetic field in the transverse direction, described by Hamiltonian

$$\hat{H}_{\text{Heis}} = -J \sum_{\langle i,j \rangle} \hat{S}_z^{(i)} \hat{S}_z^{(j)} - gJ \sum_i \hat{S}_x^{(i)} \ , \tag{16}$$

Boson sampling. There is strong evidence that simulating multi-mode linear optical devices is hard. The problem has been formalized and can be stated as follows: consider a linear optical device with M modes and in which N single photons are injected in the first $N \leq M$ modes. The photons are detected in the output modes with occupation numbers that vary from repetition to repetition of the experiment. The task is to sample from this output distribution and, under the assumption that $N \ll M$ and that the linear optical device has been chosen at random (see [AA14] for details), together with some common theoretical conjectures, it has been shown that such a task is classically hard to perform. Such devices are composed of two kinds of optical elements: single-mode phase shifters and two-mode beam splitters. Here we consider the possibility of implementing the same dynamics not with optical systems, but using qubits. This approach may find utility for example in testing computational complexity conjectures, if advanced qubit-based quantum computers come to fruition before advanced dedicated bosonic devices. A recent work discussed mappings to qubits for simulating quantum optics [Sab20].

In contrast to the other examples in this section, the dynamics of boson sampling is described in a stroboscopic way with layer-by-layer unitary operations, instead of being described by the time evolution of a large Hamiltonian. Nevertheless, the results of the previous sections can be readily applied when we describe the unitary operations in terms of their generators, in practice providing the effective Hamiltonians governing the evolution in each optical element. For single-mode phase shifter one has:

$$\hat{h}_{\text{p.s.}} = \hat{a}_i^\dagger \hat{a}_i \tag{17}$$

while for two-mode beam splitter one has:

$$\hat{h}_{\text{b.s.}} = \hat{a}_i^\dagger \hat{a}_j + \hat{a}_j^\dagger \hat{a}_i \tag{18}$$

with indices i, j labelling the different optical modes.

Note that this implementation is different from the previous Hamiltonian simulation examples, because the goal is to implement

$$\hat{U}_{\text{Boson Sampling}} = \exp(-i\theta_R \hat{h}_R) \exp(-i\theta_{R-1} \hat{h}_{R-1}) \cdots \exp(-i\theta_1 \hat{h}_1) \tag{19}$$

where $\hat{h}_1, \cdots, \hat{h}_R$ are the ordered list of effective Hamiltonians for each gate considered. Effectively, we produce quantum circuits that, after encoding the problem to qubits, performs a first-order Trotterization on each separate unitary.

VII. FULL COMPOSITE HAMILTONIAN RESULTS

Supplementary Figures 3 – 7 show two-qubit entangling gate resource requirements relative to SB, respectively for the one-dimensional QHO, spin-s transverse Heisenberg model, Bose-Hubbard model, boson sampling problem, and Franck-Condon problem. The latter four cases correspond to an arbitrary number of particles or modes. The bosonic Hamiltonians are plotted up to $d = 16$ and the Heisenberg model up to $s = \frac{7}{2}$. Scenarios A through D (defined in the main text), to which each combination d and problem class belong, are given in the captions. As stated in the main text, results for converting between Gray and SB are omitted when they are no better than Gray-only and SB-only. Additionally, results for expanding and re-compacting ("All with compacting") are omitted if unary-only is not better than all the compact schemes. Note that many of the "SB & Gray" results included in the plots are only marginally ($< 1\%$) superior to the SB-only and Gray-only results.

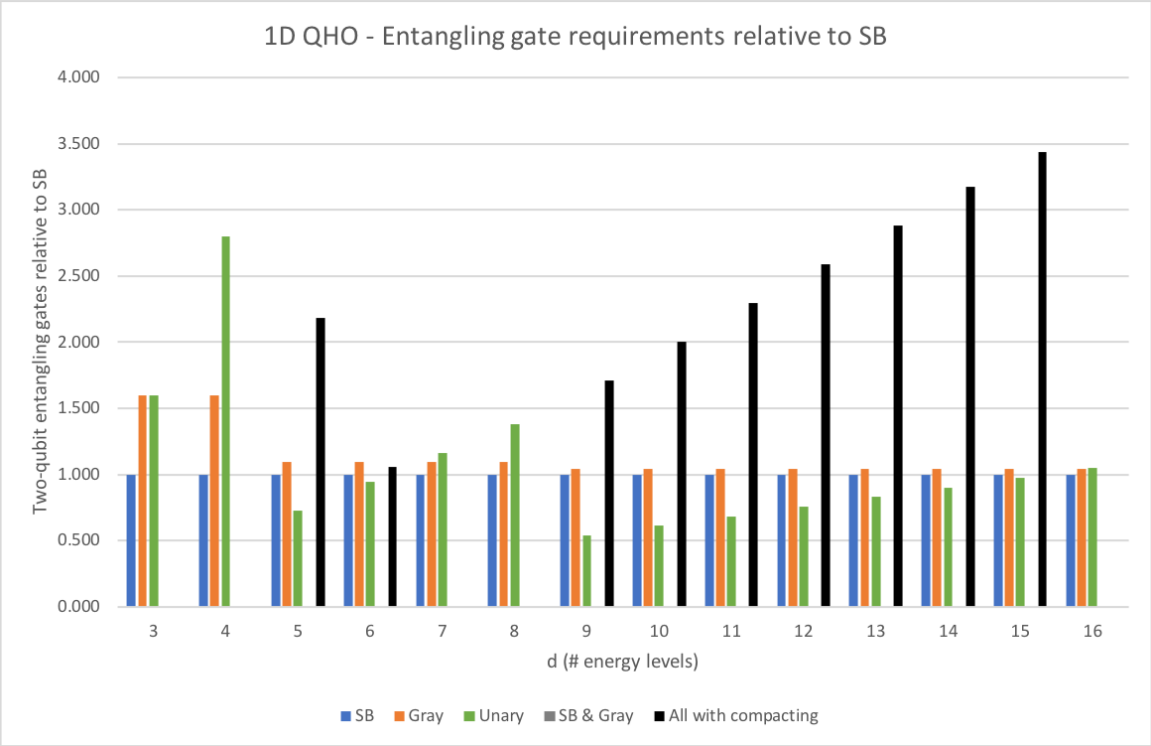

Supplementary Figure 3. Two-qubit entangling gate resource requirements, relative to SB, for the one-dimensional QHO. In order from d=3 through 16, the encoding *scenarios* are respectively *A, A, D, D, A, A, D, D, D, D, D, D, D, A*.

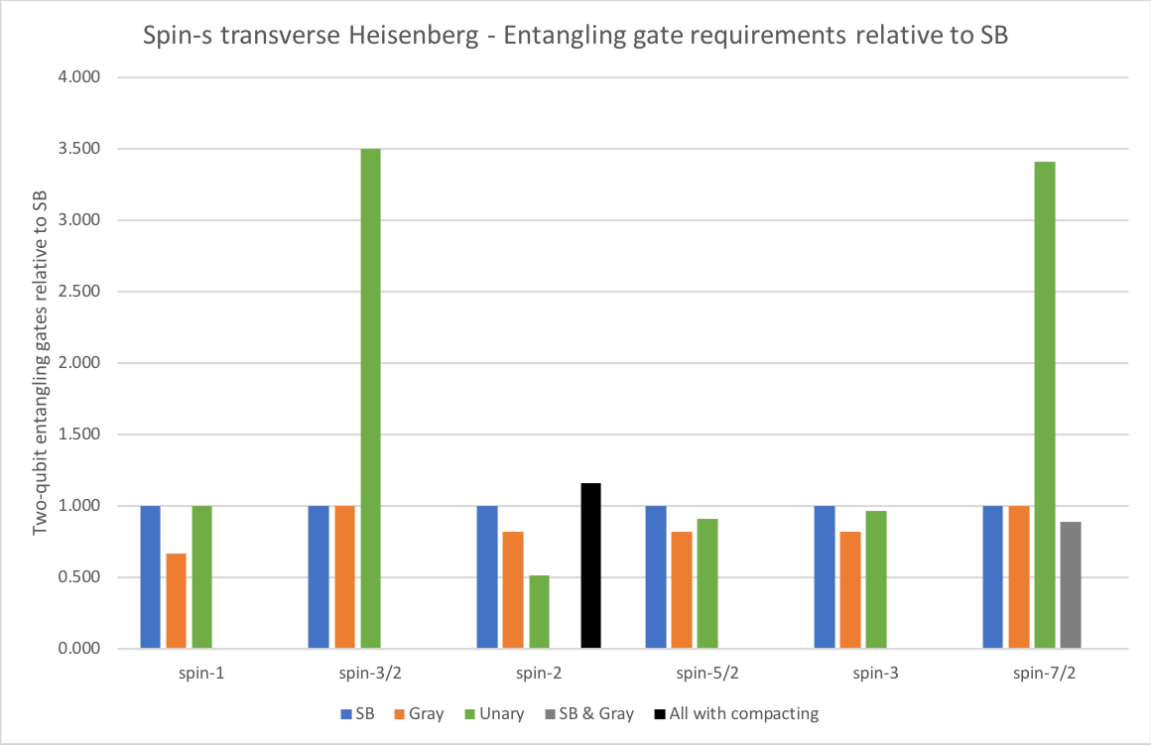

Supplementary Figure 4. Two-qubit entangling gate resource requirements, relative to SB, for a spin-s transverse Heisenberg model with an arbitrary number of particles N. In order from s=1 through $\frac{7}{2}$, the encoding *scenarios* are respectively *A, A, D, A, A, B*.

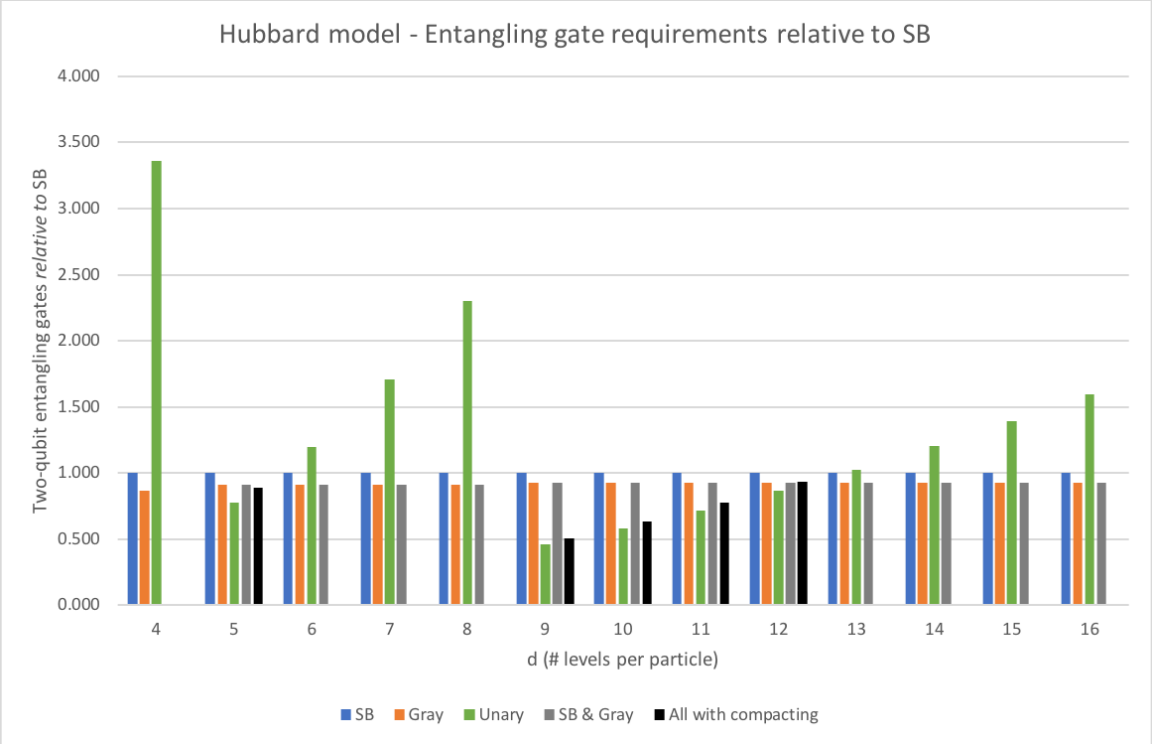

Supplementary Figure 5. Two-qubit entangling gate resource requirements, relative to SB, for a Bose-Hubbard model with an arbitrary number of particles N. In order from d=4 through 16, the encoding *scenarios* are respectively *A, C, B, B, B, C, C, C, D, B, B, B, B.*

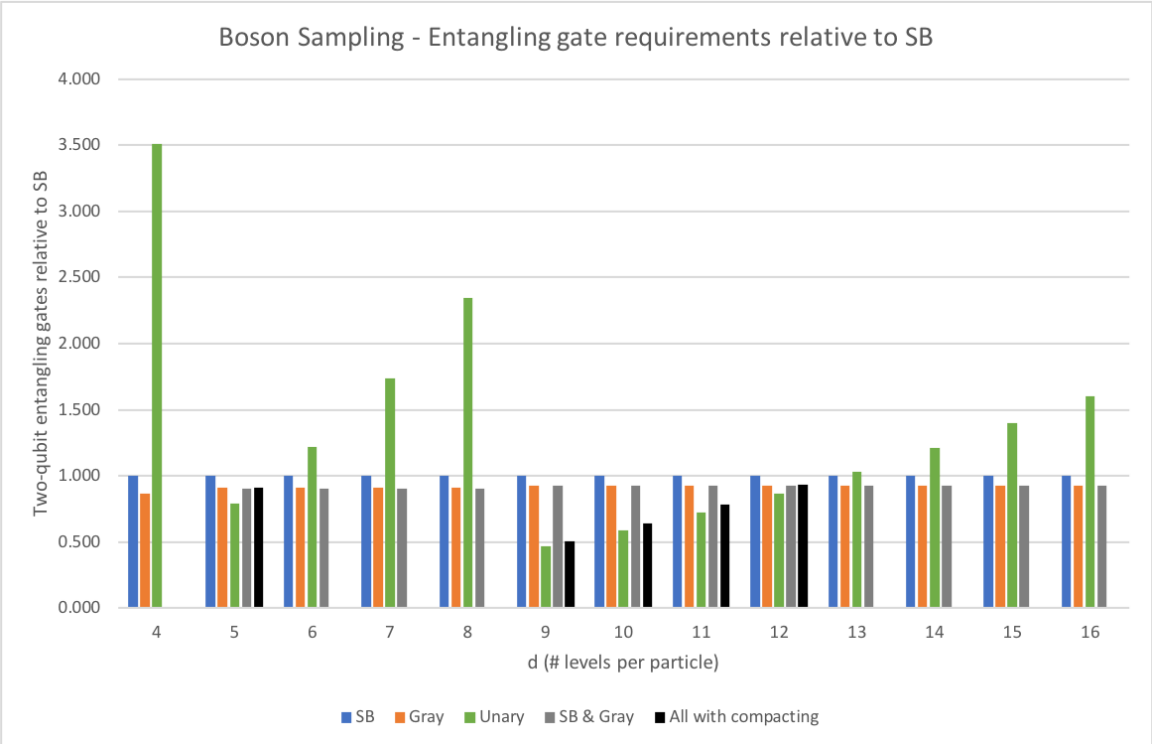

Supplementary Figure 6. Two-qubit entangling gate resource requirements, relative to SB, for a digital quantum simulation of boson sampling, with an arbitrary number of photonic modes. In order from d=4 through 16, where $d-1$ is the maximum number of photons per optical mode, the encoding *scenarios* are respectively *A, D, B, B, B, C, C, C, D, B, B, B, B.*

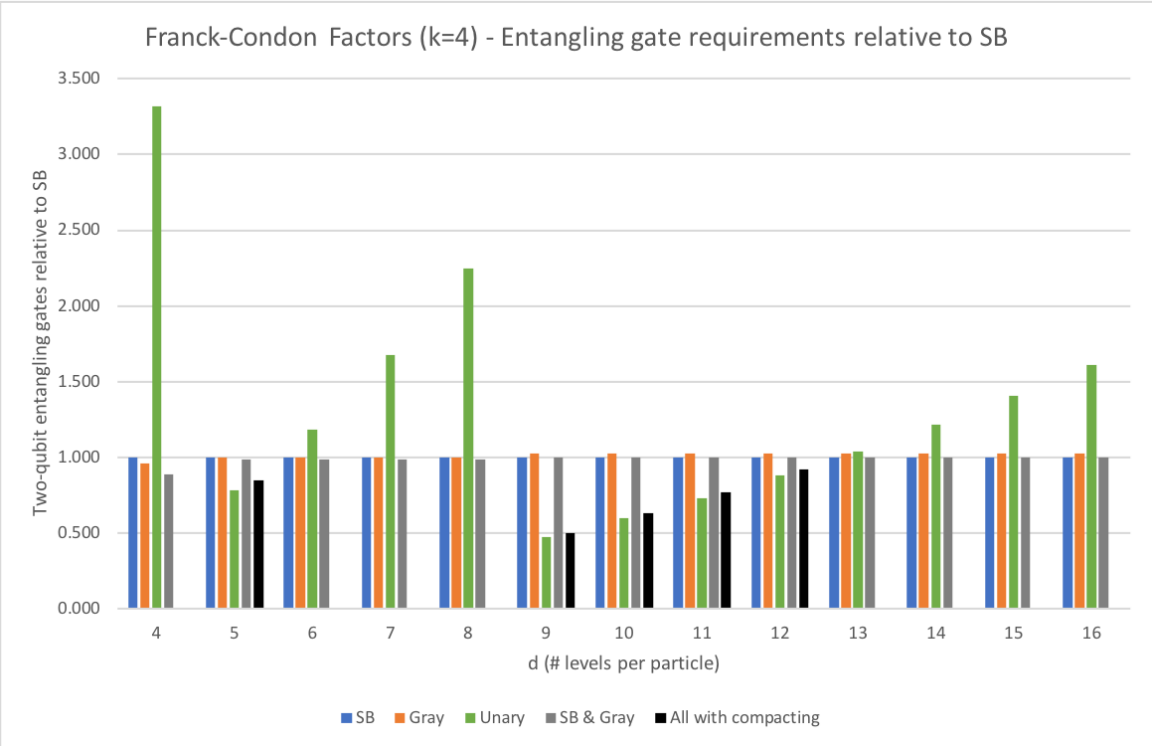

Supplementary Figure 7. Two-qubit entangling gate resource requirements, relative to SB, for implementing a Franck-Condon Hamiltonian of a molecule of arbitrary size, assuming k=4. In order from d=4 through 16, the encoding *scenarios* are respectively *B, C, B, B, B, C, C, C, C, B, B, B, B.*

[AA14] Scott Aaronson and Alex Arkhipov. The computational complexity of linear optics. In *Research in Optical Sciences*. OSA, 2014.

[BDZ08] Immanuel Bloch, Jean Dalibard, and Wilhelm Zwerger. Many-body physics with ultracold gases. *Rev. Mod. Phys.*, 80:885–964, Jul 2008.

[BKM18] Adi Botea, Akihiro Kishimoto, and Radu Marinescu. On the complexity of quantum circuit compilation. In *The Eleventh International Symposium on Combinatorial Search (SoCS 2018)*. AAAI Publications, 2018.

[BSW+19] Fabian Böttcher, Jan-Niklas Schmidt, Matthias Wenzel, Jens Hertkorn, Mingyang Guo, Tim Langen, and Tilman Pfau. Transient supersolid properties in an array of dipolar quantum droplets. *Phys. Rev. X*, 9:011051, Mar 2019.

[CPI+19] L. Chomaz, D. Petter, P. Ilzhöfer, G. Natale, A. Trautmann, C. Politi, G. Durastante, R. M. W. van Bijnen, A. Patscheider, M. Sohmen, M. J. Mark, and F. Ferlaino. Long-lived and transient supersolid behaviors in dipolar quantum gases. *Phys. Rev. X*, 9:021012, Apr 2019.

[FWGF89] Matthew P. A. Fisher, Peter B. Weichman, G. Grinstein, and Daniel S. Fisher. Boson localization and the superfluid-insulator transition. *Phys. Rev. B*, 40:546–570, Jul 1989.

[HGP+15] Joonsuk Huh, Gian Giacomo Guerreschi, Borja Peropadre, Jarrod R. Mcclean, and Alán Aspuru-Guzik. Boson sampling for molecular vibronic spectra. *Nature Photonics*, 9(9):615–620, 2015.

[HNRB10] Joonsuk Huh, Michael Neff, Guntram Rauhut, and Robert Berger. Franck-Condon profiles in photodetachment-photoelectron spectra of and based on vibrational configuration interaction wavefunctions. *Molecular Physics*, 108(3-4):409–423, Feb 2010.

[Huh11] Joonsuk Huh. *Unified Description of Vibronic Transitions with Coherent States.* PhD thesis, Goethe Univ. Frankfurt, 2011.

[HW17] Li Huang and Lei Wang. Accelerated monte carlo simulations with restricted boltzmann machines. *Physical Review B*, 95(3), Jan 2017.

[LDML08] Jonas Larson, Bogdan Damski, Giovanna Morigi, and Maciej Lewenstein. Mott-insulator states of ultracold atoms in optical resonators. *Phys. Rev. Lett.*, 100:050401, Feb 2008.

[Lev08] Malcolm H. Levitt. *Spin Dynamics: Basics of Nuclear Magnetic Resonance, 2nd edition.* Wiley, 2008.

[LGHL18] Yongqiang Li, Andreas Geißler, Walter Hofstetter, and Weibin Li. Supersolidity of lattice bosons immersed in strongly correlated rydberg dressed atoms. *Phys. Rev. A*, 97:023619, Feb 2018.

[LKC06] Josep M. Luis, Bernard Kirtman, and Ove Christiansen. A variational approach for calculating Franck-Condon factors including mode-mode anharmonic coupling. *The Journal of Chemical Physics*, 125(15):154114, Oct 2006.

[LSGB+16] R. Lora-Serrano, D.J. Garcia, D. Betancourth, R.P. Amaral, N.S. Camilo, E. Estévez-Rams, L.A. Ortellado G.Z., and P.G. Pagliuso. Dilution effects in spin 7/2 systems. the case of the antiferromagnet GdRhIn 5. *Journal of Magnetism and Magnetic Materials*, 405:304–310, 2016.

[MMS+19] Sam McArdle, Alexander Mayorov, Xiao Shan, Simon Benjamin, and Xiao Yuan. Digital quantum simulation of molecular vibrations. *Chem. Sci.*, 10:5725–5735, 2019.

[MR15] Patrick Meier and Guntram Rauhut. Comparison of methods for calculating franck–condon factors beyond the harmonic approximation: how important are duschinsky rotations? *Molecular Physics*, 113(23):3859–3873, 2015.

[MSAH18a] Alexandru Macridin, Panagiotis Spentzouris, James Amundson, and Roni Harnik. Digital quantum computation of fermion-boson interacting systems. *Phys. Rev. A*, 98:042312, Oct 2018.

[MSAH18b] Alexandru Macridin, Panagiotis Spentzouris, James Amundson, and Roni Harnik. Electron-phonon systems on a universal quantum computer. *Phys. Rev. Lett.*, 121:110504, Sep 2018.

[MSK+17] Jarrod R. McClean, Kevin J. Sung, Ian D. Kivlichan, Yudong Cao, Chengyu Dai, E. Schuyler Fried, Craig Gidney, Brendan Gimby, Pranav Gokhale, Thomas Häner, Tarini Hardikar, Vojtech Havlicek, Oscar Higgott, Cupjin Huang, Josh Izaac, Zhang Jiang, Xinle Liu, Sam McArdle, Matthew Neeley, Thomas O'Brien, Bryan O'Gorman, Isil Ozfidan, Maxwell D. Radin, Jhonathan Romero, Nicholas Rubin, Nicolas P. D. Sawaya, Kanav Setia, Sukin Sim, Damian S. Steiger, Mark Steudtner, Qiming Sun, Wei Sun, Daochen Wang, Fang Zhang, and Ryan Babbush. Openfermion: The electronic structure package for quantum computers, 2017.

[PR17] Taras Petrenko and Guntram Rauhut. A general approach for calculating strongly anharmonic vibronic spectra with a high density of states: The $\tilde{X}2B1 \leftarrow \tilde{X}1A1$ photoelectron spectrum of difluoromethane. *Journal of Chemical Theory and Computation*, 13(11):5515–5527, 2017.

[Sab20] Carlos Sabín. Digital quantum simulation of linear and nonlinear optical elements. *Quantum Reports*, 2(1):208–220, mar 2020.

[SH19] Nicolas P. D. Sawaya and Joonsuk Huh. Quantum algorithm for calculating molecular vibronic spectra. *The Journal of Physical Chemistry Letters*, 10(13):3586–3591, 2019.

[SJG10] Rashi Sachdeva, Sonika Johri, and Sankalpa Ghosh. Cold atoms in a rotating optical lattice with nearest-neighbor interactions. *Phys. Rev. A*, 82:063617, Dec 2010.

[Sto05] N.J. Stone. Table of nuclear magnetic dipole and electric quadrupole moments. *Atomic Data and Nuclear Data Tables*, 90(1):75–176, 2005.

[TLF+19] L. Tanzi, E. Lucioni, F. Famà, J. Catani, A. Fioretti, C. Gabbanini, R. N. Bisset, L. Santos, and G. Modugno. Observation of a dipolar quantum gas with metastable supersolid properties. *Phys. Rev. Lett.*, 122:130405, Apr 2019.